Electroweak asymmetries from SLD

G. Bellodi[a]

[a]Physics Department, Queen Mary University of London,
Mile End Road, London E1 4NS, United Kingdom

We present a summary of the results on electroweak asymmetries performed by the SLD experiment at the Stanford Linear Collider (SLC). Most of these results are final and are based, unless otherwise stated, on the full 1993-1998 data set of approximately 550,000 hadronic decays of Z^0 bosons, produced with an average electron beam polarization of 73%.

1. Introduction

In the Standard Model, the vertex factor for the weak neutral current interaction in the $Z^0 \to f\bar{f}$ process is given by:

$$\frac{-ig}{2\cos\theta_W}\gamma^\mu(g_V^f - g_A^f\gamma^5), \tag{1}$$

where g is the electroweak coupling constant, θ_W is the electroweak mixing angle, g_V^f and g_A^f are the vector and axial-vector couplings respectively. These latter ones can also be expressed in terms of the left- and right-handed couplings, and receive exact specifications by the Standard Model:

$$g_L^f = I_3 - Q\sin^2\theta_W\,, \quad g_R^f = Q\sin^2\theta_W. \tag{2}$$

Here I_3 denotes the third component of the weak isospin and Q is the fermion charge.
The strength of these couplings can be determined experimentally by the measurement of two physical observables: the amount of parity violation A_f in the coupling of the Z^0 to the fermion f:

$$A_f = \frac{2g_V^f g_A^f}{(g_V^f)^2 + (g_A^f)^2} = \frac{(g_L^f)^2 - (g_R^f)^2}{(g_L^g)^2 + (g_R^f)^2}, \tag{3}$$

and the rate of production of quark flavour f as a fraction of the total hadronic width (R_f):

$$R_f = \frac{\Gamma(Z^0 \to f\bar{f})}{\Gamma(Z^0 \to \ hadrons)} \propto (g_L^f)^2 + (g_R^f)^2. \tag{4}$$

The Standard Model predictions for A_f for all the fermion families are given in Table 1. The lepton asymmetries are sensitive probes of the electroweak mixing angle $\sin^2\theta_W$. For the quarks, the b system is particularly interesting. Since $(g_L^b)^2 \simeq 30(g_R^b)^2$, the R_b and A_b measurements are complementary in the complete determination of the $Zb\bar{b}$ vertex. Precise measurements of A_f for the different fermions test the universality of the theory between the generations within each family.
The Born level differential production cross section for $e^+e^- \to Z^0 \to f\bar{f}$ with longitudinally polarized electrons and unpolarized positrons is:

$$\frac{d\sigma}{d\cos\theta_f} \sim (1 - A_eP_e)(1 + \cos^2\theta_f) + 2A_f(A_e - P_e)\cos\theta_f, \tag{5}$$

where θ_f is the polar angle of the outgoing fermion f with respect to the incident electron beam direction and P_e is the electron beam polarization. It is possible to measure A_f by forming asymmetries in $\cos\theta_f$ and P_e.
The forward-backward asymmetry is defined as:

$$A_{FB}^f = \frac{\sigma_F^f - \sigma_B^f}{\sigma_F^f + \sigma_B^f} = \frac{3}{4}A_eA_f, \tag{6}$$

(where F refers to $\cos\theta_f > 0$), and it depends from both the initial and the final-state couplings. With a polarized beam it is possible to isolate A_f alone by forming the left-right forward-backward asymmetry:

$$\tilde{A}_{FB}^f = \frac{(\sigma_{FL}^f - \sigma_{BL}^f) - (\sigma_{FR}^f - \sigma_{BR}^f)}{(\sigma_{FL}^f + \sigma_{BL}^f) + (\sigma_{FR}^f + \sigma_{BR}^f)} = \frac{3}{4}|P_e|A_f. \tag{7}$$

Table 1
Coupling parameters and asymmetries for the fermion families for $\sin^2\theta_W = 0.23$.

Fermions	I_3	Q	g_L^f	g_R^f	A_f	$\delta A_f/\delta\sin^2\theta_W$
ν_e,ν_μ, ν_τ	1/2	0	0.5	0	1	0
e, μ, τ	-1/2	-1	-0.27	-0.23	0.155	-7.9
u, c, t	1/2	2/3	0.35	-0.16	0.667	-3.5
d, s, b	-1/2	-1/3	-0.43	0.08	0.935	-0.6

Here the dependence on the initial coupling disappears, allowing a direct measurement of the final state coupling parameter A_f, with a statistical advantage of $(P_e/A_e)^2 \sim 25$ compared to A_{FB}.
The initial state coupling is determined most precisely via the left-right cross section asymmetry:

$$A_{LR} = \frac{1}{P_e}\frac{\sigma_L - \sigma_R}{\sigma_L + \sigma_R} = A_e, \tag{8}$$

which gives a very precise measurement of the electroweak mixing angle, due to $\delta A_e \sim 8\delta\sin^2\theta_W$ (see Table 1).

2. The SLD experiment at SLC

The SLAC Linear Collider (SLC) delivered excellent performance in the 1997-98 run, reaching peak luminosities of 3×10^{30} cm^{-2}s^{-1}. Approximately 350,000 Z^0 decays were collected, more than doubling the SLD data set to a total of around 550,000 for 1993-1998.
A general description of the SLD detector can be found in [1]. Here we will only mention several of the unique features that allowed SLD to perform many competitive electroweak and heavy flavour measurements:

- a highly longitudinally polarized (average $\sim 73\%$) electron beam;
- a small and stable beam spot (1.5μm$\times0.8\mu$m$\times700\mu$m), essential for identifying weakly-decaying heavy mesons;
- good particle identification provided by the Čerenkov Ring Imaging Detector (CRID) [2];
- a high precision 3D CCD-based pixel vertex detector [3], which allows determination of the interaction point to a 4μm$\times4\mu$m$\times11\mu$m precision, and provides impact parameter resolution of 7.7$\times$9.6μm ($r\phi \times rz$) for high-momentum tracks.

Table 2
History of polarization measurements at SLD [8].

Year	Z^0 stat	$\mathcal{P}_e$	$\delta\mathcal{P}_e/\mathcal{P}_e$
1992	11K	$.224 \pm .006$	2.7%
1993	50K	$.630 \pm .011$	1.7%
1994-5	100K	$.772 \pm .005$	0.7%
1996	50K	$.762 \pm .004$	0.5%
1997-8	343K	$.729 \pm .004$	0.5%

2.1. Polarization Measurement

The electron polarization plays a crucial part in the SLD physics program. The polarization is primarily measured with a Compton polarimeter. The electron beam is brought into collision with a circularly polarized laser beam 33m downstream from the IP. From the asymmetry in the Compton scattering cross sections with different spin configurations, it is possible to extract the electron polarization. Two additional counters are used to cross-check the measurement [4–7]. Data from the Compton polarimeter is acquired continuously during normal SLC operation. Since it takes $\sim$ 3 minutes to complete a measurement, each hadron event is associated with a time-weighted polarization average of the measurements taken within an hour of the event. The year-by-year average measurements are summarized in Table 2.

The positron polarization has been measured directly with a Møller polarimeter in the End Station A and found to be ($-0.02 \pm 0.07\%$), which is consistent with zero.

3. Measurement of A_{LR}

The A_{LR} measurement is particularly simple, since all it requires is the count of the Z hadronic events produced with left- and right-handed electron beam. This leads to the cancellation of possible systematic effects and hence to a very small systematic error.

A_{LR} is obtained from the raw asymmetry A_m according to:

$$A_{LR} = \frac{1}{\mathcal{P}_e} \frac{N_Z(L) - N_Z(R)}{N_Z(L) + N_Z(R)} = \frac{1}{\mathcal{P}_e} A_m, \tag{9}$$

where $N_Z(L)(N_Z(R))$ is the number of hadronic events produced with a left-(right-)handed electron beam. $\mathcal{P}_e$ is the luminosity-averaged electron polarization, defined as:

$$\mathcal{P}_e = (1+\xi)\frac{1}{N_Z}\sum_{i=1}^{N_Z} P_i, \tag{10}$$

where P_i is the polarization measurement associated in time with a Z^0 event and ξ is a factor that corrects for the difference in polarization between the Compton interaction point and the Z^0 production point. In 1997-1998 ξ was found to be $\xi = -0.0012 \pm 0.0010$.

Since the SLC does not run exactly at the Z^0 pole, the extracted number for $A_{LR}(A_{LR}(E_{beam}))$ has to be extrapolated to the right energy and corrected for electroweak interference ($\sim 2\%$ level correction):

$$A^0_{LR} = (1+\epsilon)A_{LR}(E_{beam}), \tag{11}$$

where A^0_{LR} is the asymmetry at the Z^0 pole.

The systematic errors of this measurement come from uncertainties in the correction factors applied and are listed in Table 3.

Combining statistical and systematic errors, the final result on A_{LR}, using the 1993-8 data set is: $A^0_{LR}(\equiv A_e) = 0.15138 \pm 0.00216$, which corresponds to a measurement of $\sin^2\theta_{eff} = 0.23097 \pm 0.00027$ [9].

4. Leptonic Coupling Asymmetries

The electron polarization allows a direct measurement of the final-state asymmetry parameter A_l for lepton l using the left-right forward-backward asymmetry on lepton final states. If lepton universality is assumed, the results for all three flavours can be combined to yield a determination of $\sin^2\theta_W^{eff}$, which in turn can be combined with the more precise result of A_{LR}, independent from it since it is based only on hadronic events (bar a very small admixture $0.3 \pm 0.1\%$ of $\tau^+\tau^-$ events).

Figure 1 shows the $\cos\theta$ distributions for e^+e^-, $\mu^+\mu^-$ and $\tau^+\tau^-$ candidates for 1997-1998 data. The numbers of selected events for this period are respectively 15K, 11K and 11K. The pre-1997 results are similar but have smaller acceptance ($|\cos\theta| \leq 0.8$). The improved acceptance of VXD3 allowed for efficient track finding up to $|\cos\theta| = 0.9$.

Results for all data sets combined, taking into account small effects due to correlations in systematic uncertainties are:

$$\begin{aligned} A_e &= 0.1544 \pm 0.0060 \\ A_\mu &= 0.142 \pm 0.015 \\ A_\tau &= 0.136 \pm 0.015. \end{aligned} \tag{12}$$

These measurements are statistically limited. Systematic errors arise from polarimetry, backgrounds, radiative corrections, $\tau^\pm$ polarization effects, incorrect charge assignment. These results are consistent with lepton universality and hence can be combined with the A_{LR} result, yielding:

$$A_l = 0.15130 \pm 0.00207, \tag{13}$$

which is equivalent to the determination

$$\sin^2\theta_W^{eff} = 0.23098 \pm 0.00026, \tag{14}$$

where the total error and correspondent systematic error (± 0.00010) are more precise than those obtained with any other technique [10].

5. Heavy Flavour Tagging at SLD

Measurements of quark couplings require selection of individual flavours from the sample of hadronic Z decays. For bottom and charm events, this is done by searching for displaced secondary vertices. The event is split into two hemispheres using the thrust axis, and a topological vertex algorithm is applied to each to identify "seed" vertices using tracks that are considered to have

Table 3
Table of systematic errors of the A_{LR} measurement.

Factor	Systematic error
Polarization measurement	0.5%
Offset due to IP effects	0.15%
Experimental and Background asymmetry	0.07%
Electroweak and beam energy correction	0.39%
Total	$0.65\% (\sigma_{syst}(A^0_{LR}) = 0.001)$

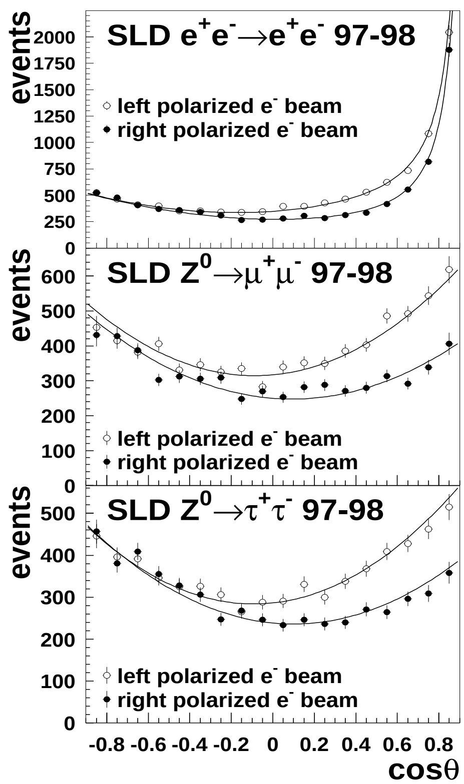

Figure 1. Distributions of the leptonic $\cos\theta$ for e^+e^-, $\mu^+\mu^-$, $\tau^+\tau^-$ candidates from the 1997-8 data set.

come from B or D meson decays. These tracks are then used to calculate a momentum and invariant mass for the hemisphere. The invariant mass is corrected for missing transverse momentum, estimated from the difference between the vertex momentum and flight direction from the IP. This quantity is shown in fig. 2. A typical bottom tag requires $M > 2$ GeV, for 98% purity and 50% efficiency.
A neural net based on the p_T-corrected vertex mass and other related variables (vertex momentum, track multiplicity and decay length) improves the performance of the tagging. Figure 3 shows the output S_{cb} of the neural net, which is ideally close to 1 for b hemispheres and close to zero for c hemispheres. A typical b tag requiring $S_{cb} > 0.75$ gave a hemisphere b-tagging efficiency of 62% and purity of 98.3%. A c tag using a cut $S_{cb} < 0.30$ gives $\epsilon_c = 18\%$ and $\Pi_c = 84\%$.

6. A_q measurements

The quark asymmetry measurements use the tags described above to select events of a particular flavour (b, c, s). In addition, we need to be able to determine which of the hemispheres contains the quark and which the antiquark. For A_b and A_c SLD has developed a number of techniques that will be described in the following.

A. A_b with Jet Charge

The method is based on the correlation between the primary quark charge and the net charge of high momentum tracks in the jet. $b\bar{b}$ events are selected by applying a vertex mass cut $M_{vtx} > 2$ GeV. The momentum-weighted track

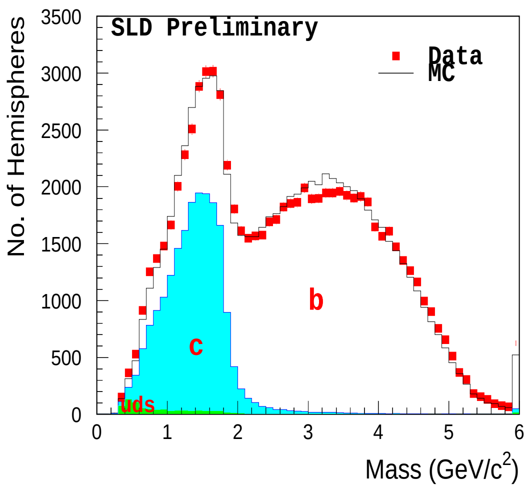

Figure 2. Distribution of the p_t-corrected mass.

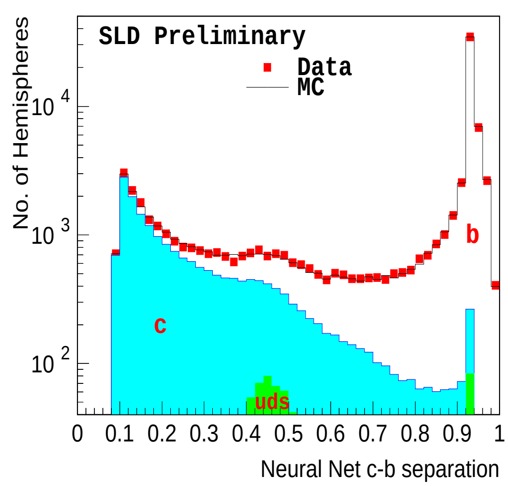

Figure 3. Distribution of the neural net b-c separation variable S_{cb} comparing data and Monte Carlo.

charge is calculated from:

$$Q = \sum_{tracks} q_i \cdot sign(\vec{p}_i \cdot \hat{T})|(\vec{p}_i \cdot \hat{T})|^{\kappa}, \qquad (15)$$

where q_i and $\vec{p}_i$ are the charge and momentum vector of track i, $\hat{T}$ is the thrust axis direction and κ was chosen to be 0.5 to maximise the analyzing power of the tag. The correct charge assignment probability is calibrated from data and its value, event by event, is fed into a maximum likelihood function [11]. On average this probability is $\sim$ 69%. The b purity is measured from data using the double-tag technique, whereas the background subtraction and hemisphere charge correlation are derived from the simulation. Figure 4 shows the polar angle distributions of the signed thrust axis for left-handed and right-handed electron beams. The SLD final result is: $A_b = 0.907 \pm 0.020_{stat} \pm 0.024_{syst}$.

B. A_b and A_c with a Lepton Tag

A_b and A_c can be measured by tagging bottom and charm events using their semileptonic decays. The lepton tag not only enriches the b and c quark events, but also provides quark-antiquark separation. The estimation of the correct charge assignment is based on the probabilities from the Monte Carlo for the candidate lepton to be from various physical sources: $b \to l$, $b \to c(\bar{c}) \to l$, $c \to l$ or light hadron and misidentified leptons. Besides the conventional total and transverse momenta, the vertex mass and other vertexing variables are used to improve the lepton source classification. The variable L/D in particular, which represents the lepton longitudinal position along the vertex axis relative to the secondary vertex location, has helped to discriminate between b direct ($b \to l$) and cascade ($b \to c(\bar{c}) \to l$) decays. Its distribution is shown in fig. 5: direct decays tend to have values of L/D < 1 while cascade decays should have L/D > 1. Clearly, there is good separation in this variable.
In the multivariate muon analysis, A_b and A_c are determined simultaneously from a maximum likelihood fit. In the electron analysis a requirement

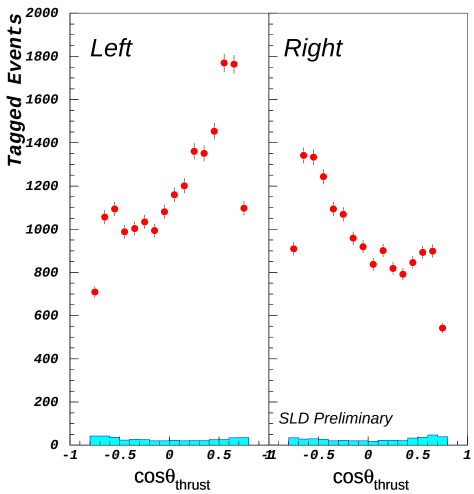

Figure 4. Polar angle distributions of the signed thrust axis for left-handed and right-handed electron beams for the jet charge analysis. Dots represent the data, and the estimated background is represented by the shaded histogram.

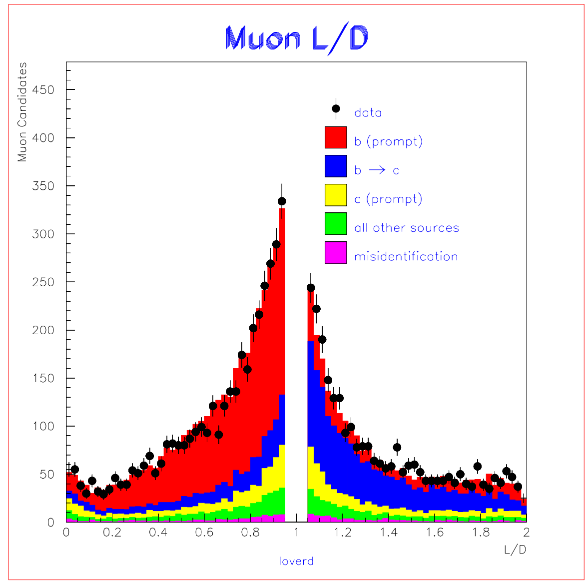

Figure 5. Tails of the L/D distribution for muons in data (dots) and Monte Carlo(histograms). Events in the central bin have been cut out, since they do not carry any discriminating information.

on the presence of a secondary vertex is applied, and hence the statistics is too low to extract a measurement of A_c. Only A_b is determined, via a neural net analysis. Major sources of systematic uncertainty were the various semileptonic branching ratios and B mixing rates, taken from the LEP combined fit results [12].
Final results are: $A_b = 0.924 \pm 0.030_{stat} \pm 0.023_{syst}$ and $A_c = 0.589 \pm 0.055_{stat} \pm 0.053_{syst}$.

C. A_b and A_c with a Vertex/Kaon Tag

The most precise A_b and A_c measurements at SLD are based on a novel quark charge assignment technique, using the vertex charge and identified kaon charge.
$b\bar{b}$ and $c\bar{c}$ events are selected by applying cuts on the S_{cb} separation variable (see fig. 3): a b tag requires $S_{cb} > 0.9$ and $M_{vtx} < 7$ GeV, and the c tag requires $S_{cb} < 0.4$ and a momentum sum of all secondary tracks >5 GeV/c. A clean reconstruction of the secondary vertex charge, improved by the inclusion in the calculation of Vertex Detector track segments alongside fully fitted tracks, tags the heavy quark charge (see fig. 6).

Another quark charge assignment method is to use the dominant $b \to c \to s \to K^-$ and $c \to s \to K^-$ decay chains, with CRID identified kaons. The additional contribution from this tag is found to be small for b hemispheres, but is very effective for c hemispheres. Therefore, the A_b analysis used the vertex-charge tag only, while the A_c analysis used both the vertex-charge and the kaon-charge tags (with no assignment in case of conflict between the two). Event flavour composition and quark charge assignment probability are determined simultaneously from data using a hemisphere double-tag technique (uds efficiencies and hemisphere correlations are taken from Monte Carlo, whereas world average values are

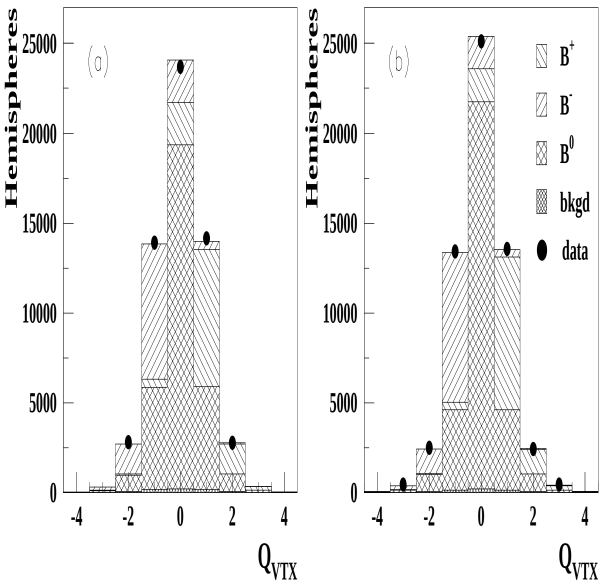

Figure 6. Vertex charge distributions for b tagged hemispheres, (a) with fully fitted tracks, and (b) including VXD track segments. The "B^0" category includes all neutral b hadrons.

assumed for R_b and R_c). Events with either hemisphere having a b tag are classified as $b\bar{b}$ events, while events with either hemisphere having a c tag or no hemisphere with a b tag are classified as $c\bar{c}$ events. Events with two hemispheres having the same charge are discarded [13].
The $b\bar{b}$ sample has a b purity of 97.5 ± 0.5% and a correct b-quark charge fraction of 81.5 ± 0.5%. The $c\bar{c}$ sample has a c purity of 83.6 ± 0.6% and a c-quark correct charge fraction of 91.2 ± 1.0%. The most significant systematic uncertainty comes from charge assignment calibration statistics. We measure: $A_b = 0.921 \pm 0.018_{stat} \pm 0.018_{syst}$ and $A_c = 0.673 \pm 0.029_{stat} \pm 0.024_{syst}$.

D. A_c with Exclusive Reconstruction

Two measurements of A_c are here performed, with the reconstruction of $D^{(*)}$ decays being not only used to select $c\bar{c}$ events, but also to tag $c(\bar{c})$ quarks with high purity. A b tag with mass requirement $M_{vtx} > 2$ GeV is used to veto $D^{(*)}$ from B decays.
The first analysis exclusively reconstructs six modes: $D^+ \to K^-\pi^+\pi^-$, $D^0 \to K^-\pi^+$ and $D^{*+} \to D^0\pi^+$ with D^0 decaying into $K^-\pi^+$, $K^-\pi^+\pi^0$, $K^-\pi^+\pi^+\pi^-$, and $K^-l^+\nu_l$ ($l = e, \mu$). The efficiency is only 4%, with however high purity and analyzing power. The final result for 1993-98 data is $A_c = 0.690 \pm 0.042_{stat} \pm 0.021_{syst}$.
The inclusive $D^{*+} \to D^0\pi_s^+$ analysis exploits the fact that a high momentum D^* in a $c\bar{c}$ jet would travel very close to the jet axis, and so would the π_s^+, due to the low Q^2. π_s candidates having momentum transverse to the jet axis $p_T^2 < 0.01$ $(\mathrm{GeV/c})^2$ are hence selected, with a signal to background ratio of 1:2 [14]. We measure: $A_c = 0.685 \pm 0.052_{stat} \pm 0.038_{syst}$.
The overlapping candidates between the two analyses are removed from the inclusive analysis for the combined A_c result.

E. A_b and A_c Summary

The individual A_b and A_c measurements were combined, taking into account systematic correlations. Due to event sample overlaps, a statistical correlation matrix was built, accounting for the different weight of each event used in the analysis [15]. For A_b the correlations obtained were: i) Lepton *vs* Jet-Q 22%, ii) Lepton *vs* Vtx-Q 15%, iii) Jet-Q *vs* Vtx-Q 32%.
The combined preliminary SLD A_b and A_c results are:

$$A_b = 0.916 \pm 0.021 \qquad (16)$$
$$A_c = 0.670 \pm 0.027$$

Figs. 7 and 8 list the SLD individual measurements and averages, along with the indirect measurements derived from the LEP A_{FB} numbers, assuming a measured A_e from the SLD and LEP combined A_{lepton} result of $A_e = 0.1501 \pm 0.0016$.

F. A_s measurement

This measurement is important to test the universality of quark couplings. Heavy quark decays

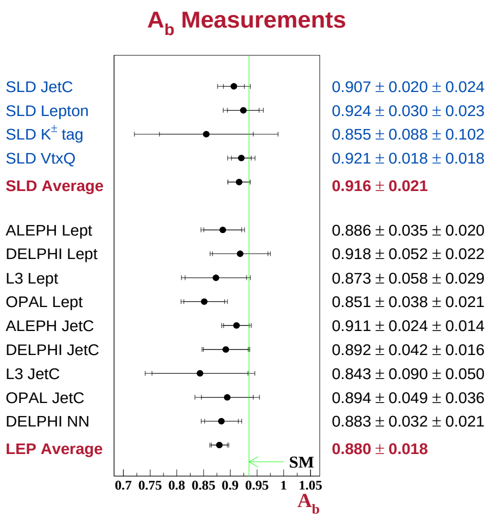

Figure 7. Summary of the SLD and indirect LEP measurements of A_b.

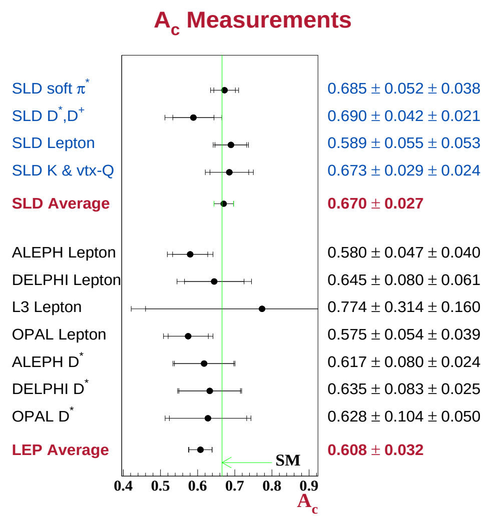

Figure 8. Summary table of the SLD and indirect LEP measurements of A_c.

are suppressed by requiring the events to contain no more than one track with normalized impact parameter in the transverse plane $d/\sigma_d > 2.5$. Charged kaons are selected with $p > 9$ GeV/c and neutral kaons with $p > 5$ GeV/c. An event is tagged as $s\bar{s}$ if one hemipshere contains a $K^{\pm}$ candidate and the other contains an oppositely charged $K^{\pm}$ (or K^0_s), with a purity of 73% (60%). The charge of the identified kaons is used to tag the sign of the initial s quark, with a correct sign probability of 97.5% for $K^+ - K^-$ events and 85% for $K^{\pm}K^0_s$. s quark $\cos\theta$ distributions for left- and right-handed electrons are shown in fig. 9. The background from ud events as well as the analyzing power are constrained from the data [16]. We measure: $A_s = 0.895 \pm 0.066_{stat} \pm 0.062_{syst}$.

7. Interpretation of the results

The SLD measurement of A_{LR} represents a benchmark for determinations of the weak mixing angle and is precise enough to put a meaningful constraint on the Higgs mass. Fig. 10a illustrates the dependence of $\sin^2\theta_W^{eff}$ on the Higgs mass. It is clear that the SLD $\sin^2\theta_W^{eff}$ result of 0.23097 prefers a low Higgs mass and that mass constraints for this value benefit from the steeper slope of the curve. By performing a χ^2 fit to the Higgs mass using the SLD measurement of the electroweak mixing angle (see fig. 10b) we calculate one-sided confidence upper limits of $m_H < 133$ GeV (95% CL) and $m_H < 205$ GeV (99% CL), in modest agreement with the current direct search lower limit from LEPII of 114.1 GeV.

The SLD data are also consistent with lepton universality. Fig. 11 summarizes the current world measurements of $\sin^2\theta_W^{eff}$. All the available leptonic data are consistent, but the results deriving from quark asymmetries provide an average (0.23230 ± 0.00029) that is 3.3σ different from the lepton asymmetries average (0.23113 ± 0.00021). This same effect shows up in the A_b "anomaly". The SLD measurements of A_b, A_c and A_s are all in good agreement with the Standard Model, and

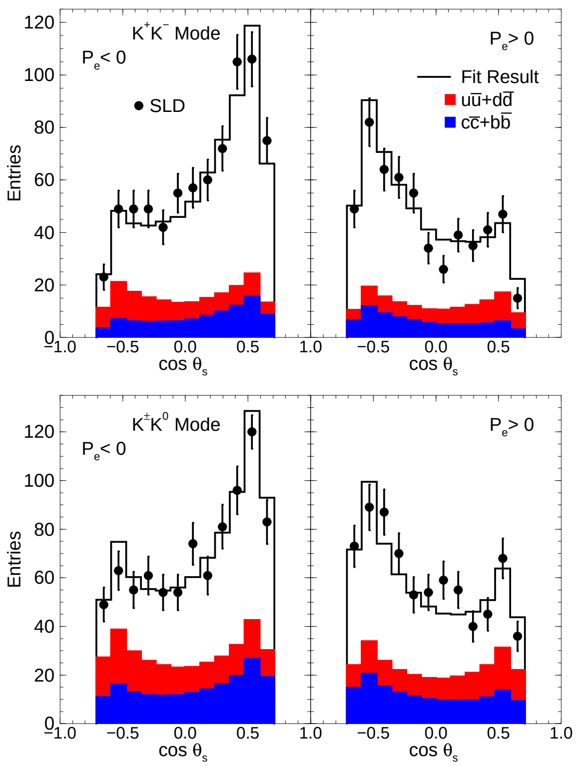

Figure 9. Distributions of the s quark $\cos\theta$ for data (points) in (a) K^+K^- events with $P_e < 0$, (b) K^+K^- events with $P_e > 0$, (c) $K^\pm K^0_s$ with $P_e < 0$ and (d) $K^\pm K^0_s$ events with $P_e > 0$. The background is indicated by the histograms.

the latter one in particular confirms quark coupling universality at the $\pm 10\%$ level. In the case of A_b and A_c, the LEP indirect measurements derived from A^b_{FB} and A^c_{FB} are lower than the SLD average at the 1.3σ and 1.5σ levels respectively. However, the derived LEP A_b average, obtained using the combined LEP and SLD average for A_e is by itself 3.1σ away from the Standard Model. A graphical representation of this is given in a TGR plane [17] (see fig. 12). Plotted on the axes are $\delta \sin^2\theta_W$ and $\delta\zeta_b$, which express the dependence on oblique and non-oblique corrections respectively at the $Zb\bar{b}$ vertex. The three 1σ-bands represent the measurements of SLD A_b, LEP A^b_{FB}

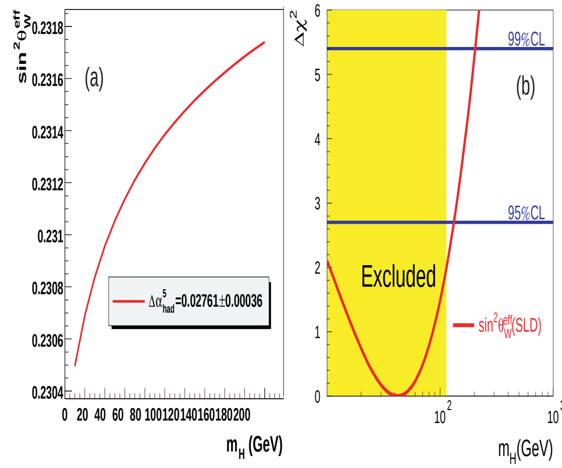

Figure 10. (a) Leading order radiative effects on $\sin^2\theta_W^{eff}$ as a function of the Higgs boson mass. (b) χ^2 curve for a fit to the Higgs mass using the SLD $\sin^2\theta_W^{eff}$ result.

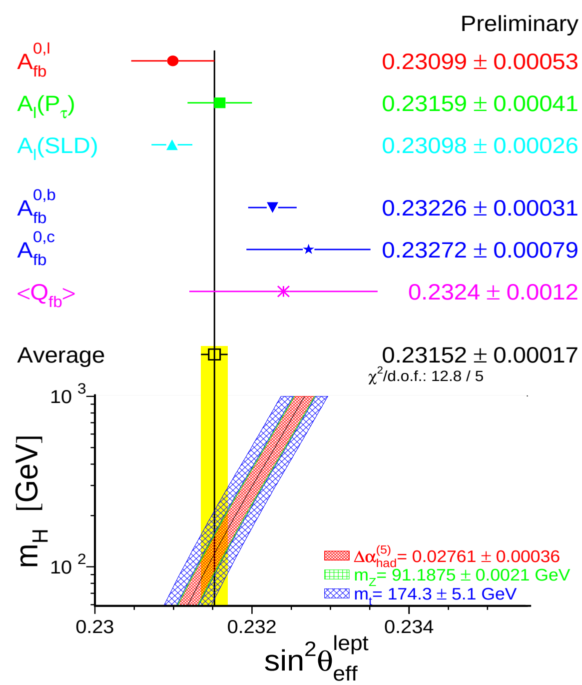

Figure 11. SLD and LEP $\sin^2\theta_W^{eff}$ results.

and SLD A_{LR}+LEP A_l and shown are the 68% and 95% confidence level ellipses of the combined fit. The origin of the plot gives the SM expectation value and the red line the dependence of this value on Higgs and top quark mass assumptions. The consistency between the various measurements and the SM is only at the 1.0% level.

A general fit for the left- and right-handed $Zb\bar{b}$

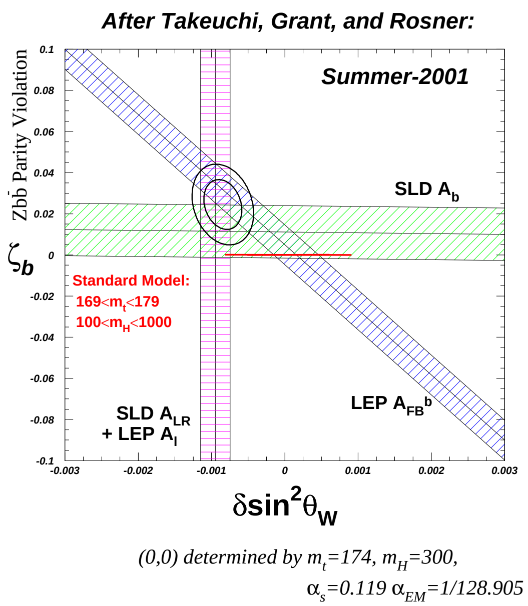

Figure 12. The $Zb\bar{b}$ coupling analysis result following Takeuchi et al.

and $Zc\bar{c}$ couplings in the SM context [18] shows a good agreement with SM predictions for the latter ones, whereas the $Zb\bar{b}$ shows a departure which mainly affects the right-handed coupling value (3σ lower than SM expectations). This is particularly difficult to accommodate because no presently known model can produce a deviation at this level.

Another more general way to look at the electroweak results is to do an S-T analysis [19] (see fig. 13). The fit ellipse is consistent with the

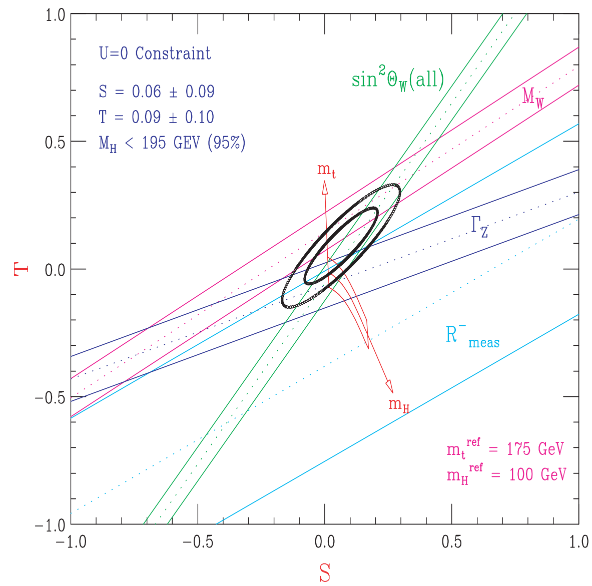

Figure 13. Global electroweak fit in the S and T plane.

banana-shaped region allowed by the SM, as long as the Higgs mass is small. It is also consistent with S = T = 0, thus excluding models predicting large deviations from these values.

8. Conclusions

The past ten years have been a "golden age" for precise electroweak measurements, and with its unique electron beam polarization and high-performance vertex detector, SLD has given important contributions.

There is generally good agreement with the Standard Model, although there are still some lingering inconsistencies with leptonic and hadronic determinations of $\sin^2\theta_W^{eff}$ and with the A_b measurement. These are still open questions that may

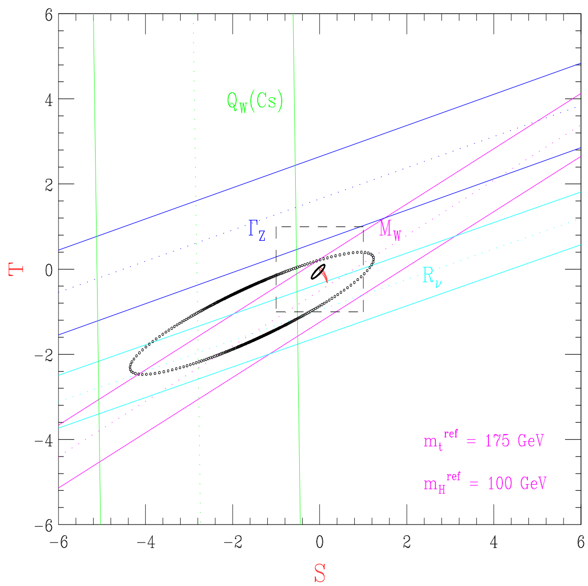

Figure 14. S-T analysis describing electroweak data available at Lepton-Photon '89.

be answered by future physics programs, if there is a return to electroweak physics at the Z pole. To conclude, we can better appreciate the success of the SLD and LEP experiments and the relevance of their legacy if we compare the present level of precision in the understanding of the subject, (see fig. 13), with the situation ten years ago, as given in fig. 14, where the current plot is shown for reference in the dashed inset.

9. Acknowledgements

We thank the personnel of the SLAC accelerator department and the technical staffs of our collaborating institutions for their outstanding efforts on our behalf. This work was supported by the U.S. Department of Energy and National Science Foundation, the UK Particle Physics and Astronomy Research Council, the Istituto Nazionale di Fisica Nucleare of Italy, the Japan-US Cooperative Research Project on High Energy Physics, and the Korea Science and Engineering Foundation.

REFERENCES

1. SLD Design Report, SLAC-Report 273 (1984).
2. K. Abe *et al.*, Nucl. Instr. Meth. **A343** 74 (1994).
3. C. J. Damerell *et al.*, Nucl. Instr. Meth. **A288** 236 (1990).
   C. J. Damerell *et al.*, Nucl. Instr. Meth. **A400** 287 (1997).
4. M. Woods, Proceedings of 12^{th} International Symposium on High Energy Spin Physics (SPIN96), ed. C. W. Jager *et al.*, 621 (1997).
5. D. Onoprienko, SLAC-Report-556 (2000).
6. E. Torrence, SLAC-Report-509 (1997).
7. D. Calloway *et al.*, SLAC-PUB-6493 (1994).
8. P. Reinertsen *et al.*, SLAC-PUB-8029 (1998).
9. T. Abe *et al.*, SLAC-PUB-8646 (2000).
   K. Abe *et al.*, Phys. Rev. Lett. **84** 5945 (2000).
10. K. Abe *et al.*, Phys. Rev. Lett. **86** 1162 (2001).
11. K. Abe *et al.*, SLAC-PUB-7886, ICHEP-PA01-179 (1998)
12. K. Abe *et al.*, SLAC-PUB-8516 (2000).
    K. Abe *et al.*, SLAC-PUB-8951 (2001), submitted to Phys. Rev. Lett.
13. K. Abe *et al.*, SLAC-PUB-8542 (2000).
    K. Abe *et al.*, SLAC-PUB-8911 (To be published.)
14. K. Abe *et al.*, Phys. Rev. **D63** 32005 (2001).
15. K. Abe *et al.*, SLAC-PUB-8211 (1999).
16. K. Abe *et al.*, SLAC-PUB-8154 (1999).
17. T. Takeuchi, A. K. Grant and J. L. Rosner, hep-ph/9409211; also in Proc. DPF 1994 Conf., Albuquerque, NM (1994), River Edge NJ: World Scientific (1995).
18. LEP Electroweak Working Group, see http://lepewwg.web.cern.ch/LEPEWWG/
19. B. Lynn, M. Peskin and R. Stuart, SLAC-PUB-3725 (1985).
    M. Peskin and T. Takeuchi, Phys. Rev. Lett. **65** 964 (1990).